

RESEARCH ARTICLE

Assessing atmospheric stability and its impacts on rotor-disk wind characteristics at an onshore wind farm

Sonia Wharton¹ and Julie K. Lundquist^{2,3}

¹ Atmospheric, Earth and Energy Division, Lawrence Livermore National Laboratory, PO Box 808, L-103, Livermore, California, 94551, USA

² Department of Atmospheric and Ocean Sciences, University of Colorado at Boulder, CUB-311, Boulder, Colorado, 80309, USA

³ National Renewable Energy Laboratory, Golden, Colorado, 80401, USA

ABSTRACT

As the average hub height and blade diameter of new wind turbine installations continue to increase, turbines typically encounter higher wind speeds, which enable them to extract large amounts of energy, but they also face challenges due to the complex nature of wind flow and turbulence in the planetary boundary layer (PBL). Wind speed and turbulence can vary greatly across a turbine's rotor disk; this variability is partially due to whether the PBL is stable, neutral or convective. To assess the influence of stability on these wind characteristics, we utilize a unique data set including observations from two meteorological towers, a surface flux tower and high-resolution remote-sensing sound detection and ranging (SODAR) instrument. We compare several approaches to defining atmospheric stability to the Obukhov length (L). Typical wind farm observations only allow for the calculation of a wind shear exponent (α) or horizontal turbulence intensity (I_U) from cup anemometers, whereas SODAR gives measurements at multiple heights in the rotor disk of turbulence intensity (I) in the latitudinal (I_u), longitudinal (I_v) and vertical (I_w) directions and turbulence kinetic energy (TKE). Two methods for calculating horizontal I from SODAR data are discussed. SODAR stability parameters are in high agreement with the more physically robust L , with TKE exhibiting the best agreement, and show promise for accurate characterizations of stability. Vertical profiles of wind speed and turbulence, which likely affect turbine power performance, are highly correlated with stability regime. At this wind farm, disregarding stability leads to over-assessments of the wind resource during convective conditions and under-assessments during stable conditions. Copyright © 2011 John Wiley & Sons, Ltd.

KEYWORDS

wind energy; planetary boundary layer; stability; turbulence intensity; wind shear

Correspondence

Sonia Wharton, Atmospheric, Earth and Energy Division, Lawrence Livermore National Laboratory, PO Box 808, L-103, Livermore, California, 94551, USA.

E-mail: wharton4@llnl.gov

Received 27 August 2010; Revised 14 February 2011; Accepted 14 April 2011

1. INTRODUCTION

As utility-scale deployment of wind energy expands, turbine sizes and generating capacities also are increasing. For example, more than 1000 wind turbines currently in operation in the USA have power-producing capacities larger than 2 MW, and new wind farms are increasingly ordering turbines on the scale of 2.5 MW or greater. Furthermore, half of all newly installed turbines in the USA in 2009 were at least 1.5 MW in capacity, with hub heights ranging from 60 to 100 m above ground level (AGL) and rotor diameters on the order of 80 m.¹ Turbines with larger capacities generally utilize higher hub heights: the Enercon E-126 6 MW turbine (Enercon GmbH, Aurich, Germany) is designed for a hub height of 135 m, with a rotor disk of 126 m.² As turbines penetrate higher altitudes, the area swept by the blades expands beyond the atmospheric surface layer (approximately the bottom 10% of the boundary layer, e.g. if the depth of the boundary layer is 1000 m, the height of the surface layer is 100 m AGL) and into the convective mixed layer with complex flows driven by buoyant turbulent mixing.³ Although mean wind velocity in the turbine rotor disk (i.e. the blade-swept area) largely determines

the amount of power that is generated, wind shear and turbulence intensity, which are measures of atmospheric stability, also appear to play a role in power output.^{4–9} Thus, defining parameters for atmospheric stability, including accurate descriptions of how wind velocity and turbulence vary across the turbine rotor disk, may prove beneficial to wind farm operations.

Stability in the lower boundary layer is largely driven by thermal gradients (called static stability) and by frictional drag, induced either along the ground surface or from wind shear aloft (called dynamic stability). For these reasons, onshore wind farms generally experience strong seasonal and diurnal patterns in the wind profile. Increased or decreased atmospheric mixing causes wind velocity in the rotor disk to deviate from the traditionally expected profile whereby pressure gradient forces cause wind speed to increase logarithmically with height from a minimum found just above the ground surface to a maximum at the top of the boundary layer. In fact, the logarithmic wind profile should be expected only when the boundary layer is near neutral.¹⁰ Near-neutral conditions exist when wind speeds are very high, vertical gradients of potential temperature are constant and the buoyancy flux is nearly non-existent. When turbulent motions are enhanced, as during daylight hours when surface heating causes air to rise (positive buoyancy), large-scale turbulent eddies reduce vertical gradients of temperature and velocity, and wind speeds are nearly uniform with low shear throughout the rotor disk. Under stable conditions, vertical motions are suppressed (negative buoyancy) and turbulence is dominated either by mechanical forces near the surface (e.g. friction along the ground surface) or high wind shear aloft [e.g. friction induced by a nocturnal low-level jet (LLJ) or gravity wave]. A stable boundary layer is characterized as having very little vertical mixing and strong gradients of temperature and velocity. Generally at night, turbulent motions are subdued because of cooling at the surface, the boundary layer is statically stable, and the air flow becomes stratified at heights encountered by the wind turbine. This decoupling can lead to high shear conditions in the rotor blade-swept area, with a shallow-depth acceleration of high-momentum air, between 100 and 300 m above the surface near the top of modern turbine rotors. Strong shear generated by these jet profiles may generate turbulence aloft.¹¹

Stability classification schemes for the planetary boundary layer (PBL) are typically based on vertical profiles of potential temperature θ [$\frac{\partial\theta}{\partial z} = \frac{\partial T}{\partial z} - \Gamma_d$, where Γ_d is the dry adiabatic lapse rate (9.8 K km^{-1})], the bulk Richardson number Ri (calculated from gradients of potential temperature and wind speed)^{12,13} or the Obukhov length L (a surface layer scaling parameter that is a function of surface heat and momentum fluxes).^{14,15} Potential temperature is useful in boundary layer studies because it normalizes the variations in temperature in an air parcel due to changes in air pressure as it rises and descends. Vertical profiles of potential temperature give the most straightforward indication of whether the boundary layer is statically stable ($\frac{\partial\theta}{\partial z} > 0$), statically unstable ($\frac{\partial\theta}{\partial z} < 0$) or neutral ($\frac{\partial\theta}{\partial z} = 0$). A complete temperature profile is, however, difficult to obtain because it requires either multiple instruments on a very tall meteorological tower or a remote-sensing platform equipped with a temperature profiler, such as a radio acoustic sounding system. Because these are very expensive, boundary-layer studies instead often rely on the surface-based Obukhov length to characterize stability, which requires a single sonic anemometer above the plant canopy or bare ground, but this approach is not ideal for wind energy applications. L does not account for low-frequency, wave-dominated turbulence nor for top-down forced boundary layers, such as those that occur during stable conditions or on nights during an LLJ;¹⁶ nor can it be applied to heights above the surface layer.^{17,18} The Obukhov length is also problematic during very stable conditions because surface fluxes may be small and intermittent¹⁹ and thus difficult to measure accurately. Therefore, a more universal yet accurate stability parameter that is based on available instrumentation is needed in the wind industry.

Wind farms typically have two means for inferring local stability, either from a dimensionless wind shear exponent α , estimated from cup anemometers at least at two measurement heights, or from turbulence intensity I (the ratio of turbulence fluctuations to mean wind speed), often from a single cup anemometer near hub height. High magnitudes of wind shear suggest a stable boundary layer whereby the turbine blades are likely to encounter strongly stratified flows across the rotor disk (e.g. much higher wind speeds at the top of the rotor than at the bottom). Very high values of shear may cause out-of-plane bending loads on the blades and may damage turbine components. Low values of wind shear indicate convective or well-mixed conditions across the rotor and a more uniform average velocity profile. Turbulence intensity is also considered a means of quantifying atmospheric stability because a stable atmosphere is generally characterized with low amounts of turbulence (except during an LLJ or gravity wave), whereas a convective atmosphere generally will be much more turbulent. High amounts of intense and highly organized (coherent) turbulence should be identified because they can impose significant aerodynamic loads on the turbine and cause fatigue damage to the turbine rotor.^{20,21}

Previous investigations of the accuracy of turbine power curves have noted a dependency of power performance on atmospheric stability through examination of the cup anemometer stability parameters, α or I . Some stability studies have focused on specific stability-related phenomena found in the lower boundary layer, including the nocturnal LLJ that produces a wind maxima^{22–24} at heights near the top of the turbine rotor.^{25–28} Other researchers have focused on the sensitivity of power curves to the wind shear exponent^{9,29–31} or to hub-height turbulence intensity.^{4,8,30,32–34} To our knowledge, this is the first study to compare such a large set of independent stability parameters, including the Obukhov length from sonic anemometry and high-resolution sound detection and ranging (SODAR) measurements of the wind shear exponent, turbulence intensity, and turbulence kinetic energy at multiple heights spanning from the bottom to top of the rotor disk. We

report high-temporal and spatial-resolution measurements of wind speed, direction, and turbulence from multiple instrument platforms, including SODAR, a pair of meteorological towers, and multiple turbines over a full year. The dependence of turbine power generation on these stability parameters will be addressed in a subsequent paper.

2. METHODS

2.1. Overview of site and available data

The data in this study were collected at a wind farm located in western North America at an elevation of near sea level, with some marine boundary layer influences. The area experiences strong land–sea temperature differences, particularly during the summer months when the land is much warmer than the coastal Pacific waters. The resulting pressure gradient produces strong onshore winds consistently from a westerly or southwesterly direction. The site has two distinct seasons: a wet, cool winter with frequent synoptic storms and a dry, warm summer with little convective storm activity due to the presence of a semi-permanent high pressure circulation over the Pacific Ocean. The landscape both upwind (called fetch) and at the wind farm is grassland on rolling hills with elevation variations of less than 100 m. Portions of the site are used for grazing.

A number of horizontal-axis, three-bladed wind turbines, with rotor diameters of approximately 80 m, are in operation at the wind farm, covering an area of approximately 6×10 km. The blades interact with the instantaneous wind speed in a disk-shaped area across heights of 40 to 120 m AGL, where 40 m is the minimum blade tip height and 120 m is the maximum blade tip height. The nacelle and power generators are located at 80 m AGL (referred to as hub height). Each turbine has a heated cup anemometer (IceFree3, NRG Systems, Hinesburg, VT) located on the end of the nacelle, providing hub-height estimates of wind speed. A subset of six leading-edge turbines was selected for analysis in this study; these turbines are located in the northwestern region of the wind farm and are all upwind of other turbines and obstacles.

The wind farm layout is shown in Figure 1 with the relative locations of the roving SODAR platform, 50 m and 80 m tall meteorological towers and subset of turbines used in this analysis. The meteorological towers are located in the upwind portion of the wind farm and are equipped with cup anemometers (#40, NRG Systems) at heights ranging from 30 to 80 m AGL. Additionally, wind direction, air temperature and barometric pressure are measured near the top of each tower. A Doppler mini SODAR (Model4000, Atmospheric Systems Corporation, Santa Clarita, CA) collected high vertical resolution, three-axis wind velocity data during most of the year-long study in the northern region of the wind farm. SODAR data enabled the calculations of a wind shear exponent, latitudinal, longitudinal and vertical turbulence intensities, and turbulence kinetic energy at 10 m intervals at heights representative of the rotor disk, as discussed in detail in the succeeding paragraphs.

In addition, the Obukhov length was calculated from three-axis wind velocity and surface heat flux measurements (WindMaster Pro 3-axis ultrasonic anemometer, Gill Instruments Ltd, Hampshire, England) from an off-site research station

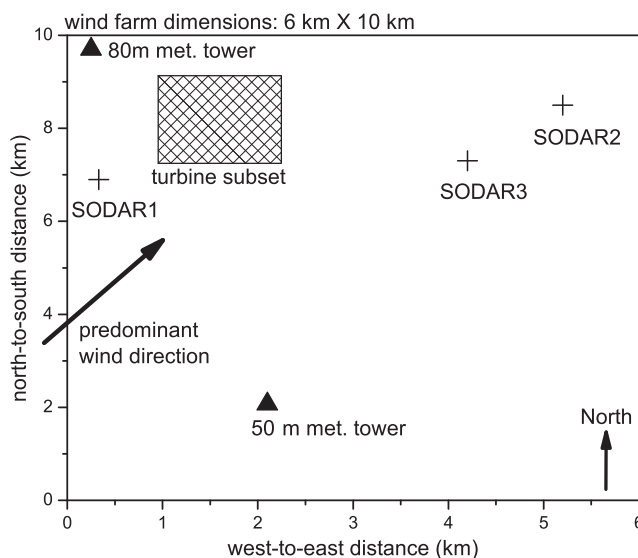


Figure 1. Illustration of the wind park and relative locations of meteorological instrumentation and turbines used in this analysis. The SODAR was a roving system, and SODAR1, SODAR2 and SODAR3 correspond to different periods.

approximately 15 km away in similar terrain. All turbine and meteorological measurements except for the Obukhov length were averaged over a 10 min period following IEC standards.³⁵ Measurements of wind speed, momentum flux and heat flux used in the Obukhov length were calculated from 30 min averages. Wind speed measurements were removed from the analysis when the following criteria were applied: standard deviation was less than 0.1 m s^{-1} , wind speed was greater than 25 or less than 0.5 m s^{-1} or wind flow was from an easterly direction and caused 'tower shadowing'. Complete instrument details are listed in Table I.

Throughout this paper, we define the wind velocities as the following: u and v are the horizontal components of wind speed, where u is the mean wind speed in the latitudinal direction (x) and v is the mean wind speed in the longitudinal direction (y); w is the mean wind speed in the vertical direction (z), and u' , v' and w' are perturbations of the instantaneous wind speed components $u(t)$, $v(t)$ and $w(t)$ from the mean wind speeds u , v and w , such that $u' = u(t) - u$. SODAR measures wind speed in three directions, whereas a cup anemometer gives only the horizontal wind speed, U . SODAR U is calculated from the square root of the sum of latitudinal and longitudinal velocities, such that $U = \sqrt{u^2 + v^2}$. In this paper, nacelle wind speed refers to the cup anemometer mounted on the nacelle hub at 80 m AGL whereas hub-height wind speed is used in broader context to include all 80 m AGL wind speed measurements from either the meteorological tower (cup anemometer), SODAR or nacelle (cup anemometer). All analyses were performed using the statistical software package ORIGIN 8 (OriginLab Corp, Northampton, MA). We report the Pearson's correlation coefficient (r) and one-way ANOVA p -value (p) at a significance level equal to the 95th confidence level ($p < 0.05$).

2.2. Evaluation of power performance

Power performance at an individual turbine was based on normalized power P_{norm} (%),

$$P_{\text{norm}} = \frac{P_{i,t}}{P_{i,\text{rated}}} \times 100 \quad (1)$$

where $P_{i,t}$ is the average amount of power (kW) generated at turbine t over a 10 min period and P_{rated} is the maximum amount of power (kW) that turbine t is potentially able to produce over a 10 min period as determined by the manufacturer. A normalized power factor of 100% indicates that a turbine is producing a power yield equal to the manufacturer's maximum power rating (e.g. 2 MW for a 2 MW rated turbine). The manufacturer's power performance data assume standard atmospheric conditions including an assumption of neutral stability and turbulence intensity of between 10% and 15%. Air density corrections for the manufacturer power curves using on-site air pressure and air temperature did not make a significant difference since this wind farm is at near sea level. Normalized power was calculated for each turbine in the subset every 10 min during the study period. We used leading-edge turbines to remove any effects that turbine-induced wakes may have on turbine power performance. Also, the distance between any upwind obstacles (e.g. a meteorological tower) and a downwind turbine was checked to verify that the turbine was no closer than four times the rotor diameter from the upwind obstacle.³⁵

2.3. Meteorological measurements and stability parameters

Vertical profiles of mean horizontal wind speed (U) (m s^{-1}) and turbulent fluctuations in the horizontal wind speed (σ_U) (m s^{-1}) were available from cup anemometers on two meteorological towers (50 and 80 m tall). Three cup anemometers were mounted on the 50 m tower at heights of 30, 40 and 50 m AGL. The 80 m tower was equipped with three cup anemometers at heights equal to 50, 60 and 80 m AGL. The cup anemometers measured horizontal wind speed at a sampling rate of 1 Hz with an accuracy of 0.3 m s^{-1} . Wind direction, barometric pressure and air temperature (T_a) were measured at 47 m AGL on the 50 m tall tower and at 77 m AGL on the 80 m tall tower. Frequent data outages in T_a , as well as the 8 km distance between the two meteorological towers, prevented the calculation of a vertical potential temperature profile to determine atmospheric stability at this site.

SODAR measurements of latitudinal, longitudinal and vertical wind speed (u , v , w) (m s^{-1}), wind direction and turbulent velocity fluctuations (σ_u , σ_v , σ_w) (m s^{-1}) were available during the majority of the study period. The SODAR transmits three high-frequency (4500 Hz) acoustic beams at a pulse width of 60 ms, and u , v and w are calculated by analyzing the frequency shift in spectral energy in the return signal from each beam.^{36,37} The wind vectors were measured at 10 m intervals from 20 to 200 m, for a total of 19 different height measurements above the ground surface, with an accuracy of 0.5 m s^{-1} . Wind speed and direction were averaged over 10 min intervals. The raw data were quality controlled according to accepted SODAR standards, e.g. those of Antoniou *et al.*³⁸ Ten minute periods that failed to meet thresholds for percentage of acceptable data ($>15\%$ bad data) and signal-to-noise ratio ($\text{SNR} < 7$) were removed. The system operated from July 2007 to May 2008 with major outages in the rainy season (November, December and January). On average, daytime (nighttime) SODAR data recovery was greater than 95% (90%) at 40 m, 90% (85%) at 80 m and 75% (83%) at 120 m AGL. The SODAR was not stationary during the study period and was moved to three site locations (SODAR1,

Table I. List of available meteorological instrumentation, variables measured and measurement heights.

	Instrument	Averaging time (min)	Location	Measurement height (m)	Measurement	No. of site locations
Wind speed	Cup anemometer	10	On site, turbine nacelle hub	80	U (m s^{-1})	6
	Cup anemometer	10	On site, 50 m tall tower	30, 40, 50	U (m s^{-1}) σ_U (m s^{-1})	1 array
	Cup anemometer	10	On site, 80 m tall tower	50, 60, 80	U (m s^{-1}) σ_U (m s^{-1})	1 array
	SODAR	10	On site, remote-sensing platform	20–200, every 10 m	u, v, w (m s^{-1}) $\sigma_u, \sigma_v, \sigma_w$ (m s^{-1})	3 (one roving system)
	3-D sonic anemometer	30	Off site, flux tower	3	$u(t), v(t), w(t)$ (m s^{-1}) u', v', w' (m s^{-1})	1
Wind direction	Wind vane	10	On site, 50 m tall tower	47	Direction ($^\circ$)	1 (partially inactive)
	Wind vane	10	On site, 80 m tall tower	77	Direction ($^\circ$)	1 (partially inactive)
	SODAR	10	On site, remote-sensing platform	20–200, every 10 m	Direction ($^\circ$)	3 (one roving system)
	3-D sonic anemometer	30	Off site, flux tower	3	Direction ($^\circ$)	1
Air temperature	Temperature sensor	10	On site, 50 m tall tower	47	T_a ($^\circ\text{C}$)	1 (partially inactive)
	Temperature sensor	10	On site, 80 m tall tower	77	T_a ($^\circ\text{C}$)	1 (partially inactive)
	Fast-response thermocouple, relative humidity sensor	30	Off site, flux tower	3	θ_v (K) RH (%)	1

SODAR2 and SODAR3) within an area of 4.8×1.5 km during the following periods: July 2007 to mid-August 2007, mid-August 2007 to September 2007, and October 2007 to May 2008. These times correspond to SODAR1, SODAR2 and SODAR3 in Figure 1, respectively.

SODAR and cup anemometer wind velocities were used to calculate a dimensionless wind shear exponent α using the power law expression,³⁹

$$U(z) = U_R \left(\frac{z}{z_R} \right)^\alpha \quad (2)$$

where U is the mean horizontal wind speed (m s^{-1}) at height z (m) and U_R is the mean horizontal wind speed (m s^{-1}) at a reference height z_R (m); by convention, height z_R is closer to the ground than z . A wind shear exponent is traditionally used to estimate variations in available wind power by height, when direct measurements of wind speed across the rotor and stability are unavailable.⁴⁰ Here, three wind shear exponents were calculated using SODAR wind speed measurements at 40, 80 and 120 m: α_{40_120} parameterizes stability across the entire rotor disk, α_{40_80} parameterizes stability across the lower half of the rotor disk and α_{80_120} parameterizes stability across the upper half of the rotor disk. A fourth, α , α_{50_80} , was calculated using the 50 and 80 m meteorological tower cup anemometer data for comparison with the SODAR shear exponent α_{40_80} . Only the periods when the wind speed was greater than the turbine cut-in speed were used to calculate α .

The wind shear exponent describes the degree of atmospheric stability on the basis of the presence (shear or no shear) and amount (low or high shear) of stratified flow but is not a direct measure of stability. Historically, a constant α -value of $1/7$ (0.14) has been used to extrapolate the wind speed taken at a reference height (usually from the nacelle anemometer) to all other heights within the blade-swept area when the wind profile is unknown. The one-seventh constant has been attributed by Rohatgi⁴¹ to von Karman's work, indicating a correspondence between wind flow in the surface layer and experimental flow over flat plates and to observations taken in the boundary layer in the 1920s by Scrase.⁴² A few studies recognized early on that serious errors can be introduced by reliance on the power law, equation (2), to estimate the wind speed profile in wind power applications.^{43–45} First, the power law has no theoretical basis for extrapolating wind speed within the boundary layer because it is not based on the basic principles of fluid mechanics and is instead derived empirically. Second, the power law should only be considered valid during neutral conditions in homogeneous, flat terrain. Finally, the power law does not acknowledge the possibility of variable wind shear across the rotor disk and its impact on turbulence.

In contrast to the wind shear exponent, which measures the amount of wind shear that may produce turbulence, turbulence intensity I (%) uses measurements of velocity fluctuations in the boundary layer to characterize stability and is a statistical descriptor of the overall level of turbulence in relation to mean wind speed. High I magnitudes indicate that a significant portion of wind energy is composed of turbulent flow, whereas low I values indicate laminar flow with less turbulence. Three component turbulence intensities can be calculated when u , v and w observations are available, as from a SODAR or sonic anemometer. These include I_u , the latitudinal turbulence intensity, I_v , the longitudinal turbulence intensity, and I_w , the vertical turbulence intensity. The first turbulence intensity, I_u , describes the relative amount of turbulence in the x direction in relation to the mean horizontal wind speed, following⁴⁶

$$I_u = \frac{\sigma_u}{U} \quad (3)$$

where σ_u (m s^{-1}) is the average standard deviation of the latitudinal velocities over a 10 min period. Likewise, turbulence intensity in the longitudinal direction is

$$I_v = \frac{\sigma_v}{U} \quad (4)$$

and turbulence intensity in the vertical direction is

$$I_w = \frac{\sigma_w}{U} \quad (5)$$

Note that calculations of longitudinal I_v or vertical I_w are not possible with a cup anemometer since the instrument measures only horizontal wind speed (U) and not the components u , v and w . We assumed here that the cup anemometer is insensitive to any changes in the vertical velocity. For the cup anemometers, turbulence intensity was determined by calculating a horizontal turbulence intensity,

$$I_{U\text{cup}} = \frac{\sigma_U}{U} \quad (6)$$

SODAR I magnitudes are not directly comparable with those from the cup anemometer because the expressions for I in equations (3)–(5) are not equal to I in equation (6). In order to directly compare the instruments, we calculated two

alternative expressions for horizontal turbulence intensity from the SODAR to include the standard deviations of u and v . Equation (7) appears to be the more accepted way to calculate SODAR I_U in the wind industry, whereby I_U is the average of the latitudinal and longitudinal turbulence fluctuations and assumes that turbulence is isotropic,

$$I_{U1\text{SODAR}} = \frac{\sum_{i=u,v} \sigma_i}{2U} \quad (7)$$

In equation (8), we followed a methodology adopted by micrometeorologists and calculated a horizontal turbulence intensity that uses the square root of the sum of turbulence in the horizontal wind components and makes no assumptions about the isotropic nature of turbulence,

$$I_{U2\text{SODAR}} = \frac{\sqrt{(\sigma_u^2 + \sigma_v^2)}}{U} \quad (8)$$

The expression for turbulence intensity in equation (8) is found in Chan⁴⁷ and is similar to derivations found in Shaw *et al.*⁴⁶ and Weber.⁴⁸ Note that equation (7) (the ‘averaging method’) and equation (8) (the ‘square-root method’) will not give identical magnitudes of I_U , even if turbulence is isotropic and σ_u equals σ_v because the two expressions for horizontal turbulence are not equal.

SODAR turbulence intensities were calculated at 10 min intervals at each of the nine measurement heights in the rotor disk. Cup anemometer I was calculated for each 10 min period at heights of 50 and 80 m using the meteorological tower cup anemometer measurements. Only periods when U was greater than the turbine cut-in speed and the standard deviations were greater than 0.1 m s^{-1} were included. These criteria excluded extremely high turbulence intensities caused by the presence of very low wind speeds and very low turbulence intensities caused by unrealistically low variance.

Related to SODAR I , turbulence kinetic energy TKE ($\text{m}^2 \text{ s}^{-2}$) was calculated from SODAR data using the three turbulence components as in equation (9),

$$\text{TKE} = \frac{1}{2}(\sigma_u^2 + \sigma_v^2 + \sigma_w^2) \quad (9)$$

TKE is a measure of the intensity of turbulence and is directly related to the transport of momentum (shear-generated turbulence that is strongest in the horizontal direction) and heat (thermal-generated turbulence in the vertical direction) through the boundary layer. Hence, TKE is the sum of all measurable sources of turbulence, both convective and mechanically generated. Here, TKE was calculated for each of the 19 SODAR measurement heights (20–200 m AGL).

TKE varies with height. For example, in an unstable boundary layer, TKE generally increases with height until a maximum is found at the level where free convection dominates. When strong winds are present or during neutral conditions, TKE may be nearly constant or may decrease slightly with height.¹⁷ During stable nighttime conditions, TKE often decreases rapidly with height from a maximum value found just above the surface. An exception to this occurs when LLJs or other elevated sources of turbulence such as breaking gravity waves are present. If nighttime TKE is generated at levels above the surface in a statically stable atmosphere and is transported downward, then this behavior suggests the presence of high wind shear and an LLJ.^{16,49–51} During an LLJ, very high wind speeds may be found at heights equal to the top of turbine rotors ($\sim 100\text{--}150 \text{ m AGL}$),⁵² but the potential for high power generation can be offset by the potential for structural turbine damage caused by intense, coherent turbulence structures just below the LLJ.²¹

Finally, a nearby university research station provided three-axis wind velocity and sensible heat flux data from a sonic anemometer and a fast-response thermocouple during the study period to calculate the stability length scale L (Obukhov length). The research station has some localized differences compared with the wind farm, including a fetch with flatter terrain and a slightly lower estimate of aerodynamic roughness length, but the winds are consistently from the same direction. Using a fast-response (output rate of 20 Hz), multi-axis sonic anemometer, measurements of mean latitudinal, longitudinal and vertical wind speed, as well as fluctuations from the mean (u' , v' and w'), offered detailed information about the structures of organized turbulence. The Obukhov length (L) (m) was used as a scaling parameter to indicate atmospheric mixing conditions in the surface layer following the Monin–Obukhov similarity theory,^{17,53–55}

$$L = -\frac{\theta_v \cdot u_*^3}{k \cdot g \cdot w' \theta'_v} \quad (10)$$

where θ_v is the virtual potential temperature (K), k is the von Karman constant (0.4), g is acceleration due to gravity (9.8 m s^{-2}), $w' \theta'_v$ is the kinematic sensible heat flux (W m^{-2}) and friction velocity, u_* (m s^{-1}) is defined from the kinematic momentum fluxes, where $u_* = (\overline{u'w'^2} + \overline{v'w'^2})^{1/4}$. Calculation of potential virtual temperature (θ_v) in the sensible heat flux eliminates the ‘apparent’ temperature variations from changes in air pressure of an air parcel as it rises

and descends. The sign of the kinematic sensible heat flux in equation (10) indicates whether the boundary layer is statically stable ($\overline{w'\theta'_v} < 0$) or statically unstable ($\overline{w'\theta'_v} > 0$). A physical interpretation of the Obukhov length is that the absolute value of L is proportional to the height (in meters) above the surface at which thermal-produced turbulence replaces shear as the dominant influence over turbulence. In contrast to the wind shear exponent, L is valid in moderately unstable or stable conditions as well as neutral boundary layers.

Equation (10) can be expressed as a non-dimensional scaling parameter z/L , where z is the height of the sonic anemometer ($z = 3.2$ m). Normalizing L by the measurement height is often performed in boundary layer studies because L magnitudes are extremely non-linear. Most of the figures in this paper use z/L to take advantage of its linearity although the stability thresholds in Table II are given for L to enable direct comparisons with other studies in the literature. L or z/L is defined as a negative quantity under convective or statically unstable conditions (the heat flux is directed away from the surface) and a positive quantity under statically stable conditions (the heat flux is directed towards the surface). L approaches infinity ($z/L \sim 0$) under neutral conditions.

2.4. Stability classifications

For each 10 min averaging period, we described the boundary layer stability conditions on the basis of the Obukhov length L , wind shear exponent α (at various heights in the rotor disk), turbulence intensity I (at 80 m AGL) and turbulence kinetic energy TKE (at 80 m AGL). We classified each 10 min period as belonging to one of five stability classes: strongly stable, stable, neutral (includes slightly stable and slightly convective), convective or strongly convective. The stability thresholds, listed in Table II, were based largely on published values, although the criteria have been modified slightly according to the range of atmospheric conditions and terrain observed at this wind farm.

The Obukhov length thresholds were based on stability classifications given by Panofsky and Dutton¹² and Stull¹⁷ and are similar to those used by van Wijk *et al.*⁵⁶ in a study of offshore wind profiles and by Sathe and Bierbooms⁵⁷ in their assessment of turbine damage induced by atmospheric stability effects. Note that our threshold for neutral conditions is less conservative than found in van Wijk *et al.*⁵⁶ and Sathe and Bierbooms⁵⁷ and includes the stability classes weakly stable and weakly convective. The wind shear exponent thresholds were based on work by van den Berg,⁸ Heald and Mahrt¹⁹ and Walter *et al.*,⁵⁸ although we defined a slightly lower threshold for strongly stable conditions ($\alpha > 0.3$). Less information is available for TKE stability criteria in wind power applications, and this paper appears to be one of the first applications of TKE in wind energy stability studies. Our TKE thresholds were based on boundary layer field campaign data found in Stull.¹⁷

Because turbulence intensity is a relative quantity, I thresholds appear to be very sensitive to the type of instrument and methodology used. The thresholds for cup anemometer I are similar to those found in Elliott and Cadogan,⁴ Rareshide *et al.*,³⁰ Kaiser *et al.*³² and Langreder *et al.*,⁵⁹ although we defined more detailed stability classes. For example, Rareshide *et al.*³⁰ defined just two stability classes on the basis of a low turbulence threshold ($I_U = 5\%$ to 11%) and a high turbulence threshold ($I_U = 11\%$ to 17%). We defined five I_U stability classes including one that describes a near-neutral atmosphere using intermediate values of turbulence intensity. Similar to what we did in our site, Elliott and Cadogan⁴ at a West Coast wind farm defined the following I_U thresholds, from low turbulence to high turbulence: 0% to 5% , 5% to 10% , 10% to 15% , and 15% to 30% .

Magnitudes of SODAR-based horizontal turbulence intensity depended on the methodology chosen to calculate turbulence in the horizontal direction. When the average of σ_u and σ_v was used to calculate σ_U , as in equation (7), we found stability thresholds for $I_{U1SODAR}$ similar to the cup anemometer I_U , although cup anemometers are known to underestimate turbulence.⁶⁰ This difference is discussed later. In contrast, the turbulence intensity magnitudes were greater when σ_U was calculated using the square root of the sum of σ_u^2 and σ_v^2 (equation (8)), and our stability criteria for $I_{U2SODAR}$ reflect this offset. We included $I_{U2SODAR}$ in this analysis because, from a micrometeorological perspective, we believe that it is the best representation of the 'actual' amount of turbulence present in the horizontal direction.

3. RESULTS

3.1. Seasonal power, wind speed and direction

This wind farm experiences two distinct wind power seasons: autumn/winter and spring/summer, as determined by the regional climatology. The autumn/winter months are dominated by synoptic-scale circulations whereas the warm season is dominated by diurnal sea-breeze circulations in response to thermal forcing. The rainy, winter season consisted of months with lower nacelle wind speeds and lower power outputs than average. Greater power production occurred during the warm season coinciding with faster nacelle winds speeds. Figure 2 shows seasonal average normalized power (a) and nacelle wind speed (b) for a single turbine, turbine #1. Average normalized power (nacelle wind speed) was 22% (4.89 m s^{-1}) in winter, 53% (8.12 m s^{-1}) in spring, 58% (8.38 m s^{-1}) in summer and 23% (5.11 m s^{-1}) in autumn. Power and wind

Table II. Stability criteria for the direct stability parameter Obukhov length and five on-site stability parameters: wind shear exponent, cup anemometer turbulence intensity, SODAR turbulence intensity (averaging method), SODAR turbulence intensity (square-root method) and turbulence kinetic energy as well as general atmospheric conditions for each stability regime.

Stability class	L (m)	α	I_{Ucup} and $I_{U1SODAR}$ (%)	$I_{U2SODAR}$ (%)	TKE ($m^2 s^{-2}$)	Boundary layer properties
Strongly stable	$0 < L < 100$	$\alpha > 0.3$	$I_U < 7\%$	$I_U < 8\%$	$TKE < 0.4$	Highest shear in swept area, nocturnal LLJ may be present, little turbulence except just below an LLJ
Stable	$100 < L < 600$	$0.2 < \alpha < 0.3$	$7 < I_U < 9\%$	$8 < I_U < 10\%$	$0.4 < TKE < 0.7$	High wind shear in swept area, nocturnal LLJ may be present, little turbulence except just below an LLJ
Neutral	$ L > 600$	$0.1 < \alpha < 0.2$	$9 < I_U < 12\%$	$10 < I_U < 13\%$	$0.7 < TKE < 1.0$	Generally strongest wind speeds throughout the blade-swept area, logarithmic wind profile
Convective	$-600 < L < -50$	$0.0 < \alpha < 0.1$	$12 < I_U < 14\%$	$13 < I_U < 20\%$	$1.0 < TKE < 1.4$	Lower wind speeds, low shear in swept area, high amount of turbulence
Strongly convective	$-50 < L < 0$	$\alpha < 0.0$	$I_U > 14\%$	$I_U > 20\%$	$TKE > 1.4$	Lowest wind speeds, very little wind shear in swept area, highly turbulent

Note that neutral conditions also include weakly stable and weakly convective. I and TKE are at 80 m; α is from 40 to 120 m.

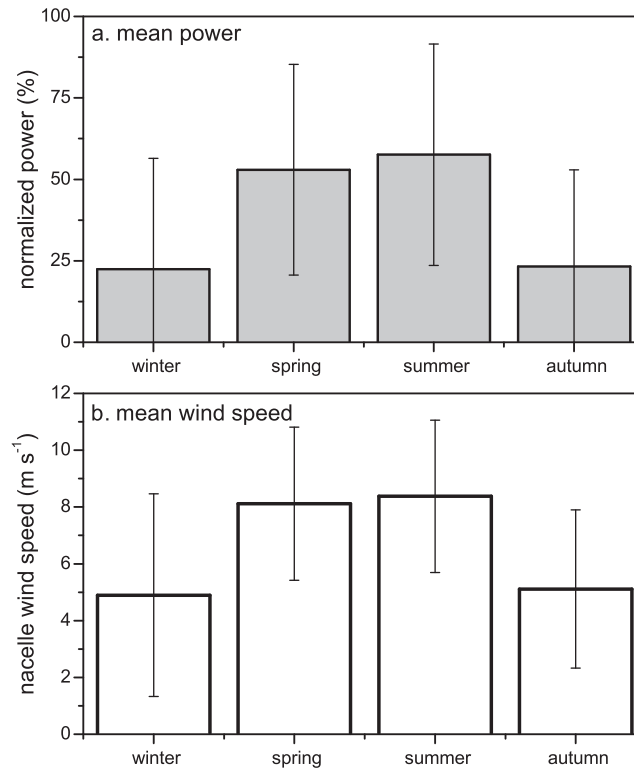


Figure 2. Seasonal mean (± 1 standard deviation) normalized power (a) and nacelle (80 m) wind speed (b) for a single turbine at the wind farm. Hub-height wind speeds during the spring and summer were on average 3 m s^{-1} higher than during the cooler months, whereas normalized power values were on average 30–35% greater.

speed conditions observed at turbine #1 were representative of the entire turbine subset during the year. Annual average normalized power was 40% for all six turbines in comparison with 39% at turbine #1.

Mean diurnal P_{norm} values are shown in Figure 3 for turbine #1. More power was generated at night than during the day, although diurnal variability varied greatly by season. The largest diurnal range in normalized power ($\Delta P_{\text{norm}} \sim 45\%$) was observed in the summer whereas diurnal variability was minimal ($\Delta P_{\text{norm}} < 15\%$) in winter and autumn and moderate ($\Delta P_{\text{norm}} \sim 25\%$) in the spring. Average nighttime (22:00–2:00 Pacific Standard Time) normalized power was 23% in winter, 63% in spring, 77% in summer and 26% in autumn. Average midday (10:00–14:00 Pacific Standard Time) normalized power was 16% in winter, 40% in spring, 32% in summer and 14% in autumn. Peak power output was observed around midnight in the summer and average P_{norm} reached 80%.

Figure 4 compares seasonal wind speed observations at 40, 80 and 120 m from the SODAR (a) and meteorological tower cup anemometers (b). Note that the highest measurement height on the meteorological tower is only 80 m. Similar to the nacelle wind speeds, SODAR and meteorological tower wind speeds were higher at night than during the day and higher during the warm season than in the cool season. The largest seasonal variability in wind speed occurred during the nighttime hours; for example, mean winter 80 m U was 5.4 m s^{-1} whereas mean summer 80 m U was nearly double, 10.1 m s^{-1} . Less seasonal variability was present during the daylight hours, although daytime wind speeds also seasonally peaked during the summer months. Although nighttime wind shear was commonly observed throughout the year, it was most prevalent during the summer months, as evident in the high-resolution SODAR data. SODAR wind speed differences approached 4 m s^{-1} between 40 and 120 m on summer nights (Figure 4(a)). Observations of wind shear at the meteorological tower (Figure 4(b)) were slightly less than wind shear measured by the SODAR. For example, average 40 to 80 m wind shear was 1.4 m s^{-1} at the meteorological tower in comparison with 2.0 m s^{-1} from the SODAR on summer nights. Unlike SODAR, the meteorological tower cup anemometers also indicated a prevalence of negative, daytime wind shear (faster wind speeds at 40 than 80 m) during spring and summer. An explanation for this is discussed next.

Over the study period, the SODAR and cup anemometers measured slight differences in mean wind speed. For example, annual mean nighttime U (80 m) was $8.5 \pm 2.8 \text{ m s}^{-1}$ from SODAR (Figure 4(a)) and $8.3 \pm 2.6 \text{ m s}^{-1}$ from the meteorological tower cup anemometer (Figure 4(b)). Annual mean daytime U (80 m) was $6.5 \pm 3.2 \text{ m s}^{-1}$ from SODAR

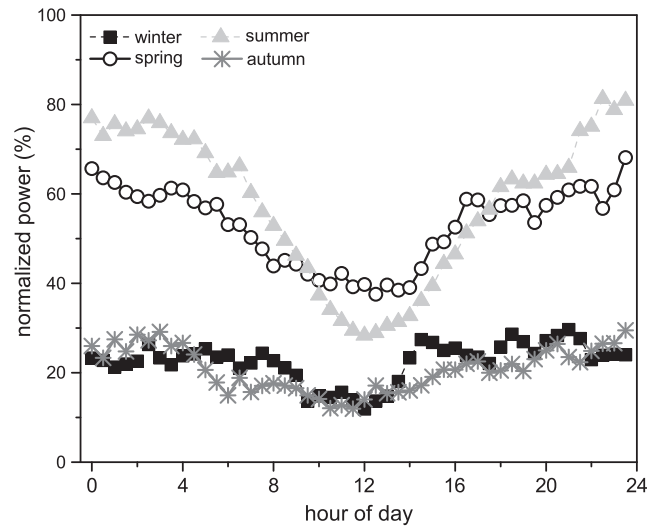


Figure 3. Mean diurnal normalized power at a single turbine by season shows large power differences at night, between spring/summer periods and winter/autumn periods, which approach 50%. Smaller power differences are also observed during the daytime hours.

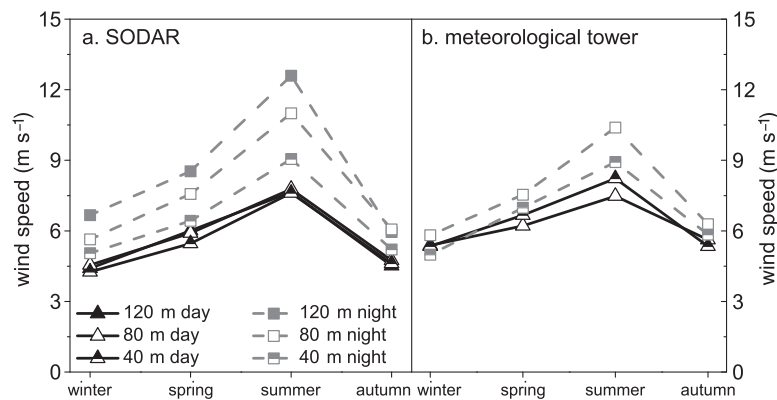


Figure 4. Mean nighttime and daytime wind speeds at 40, 80 and 120 m show a strong seasonality towards peak wind speeds in the summer and strong shear at night. Also noticeable are wind speed differences between the SODAR (a) and meteorological tower cup anemometers (b), particularly during the daytime. The meteorological tower is not instrumented at 120 m.

and $6.7 \pm 3.0 \text{ m s}^{-1}$ from the meteorological tower. The Pearson's correlation coefficient (r) between the SODAR and meteorological tower 80 m wind speeds was $r = 0.87$ during the day and $r = 0.69$ at night during the spring and summer months. The meteorological tower showed greater variability in the daytime wind speeds than the SODAR between heights of 40 and 80 m. This may be an artifact of the 8 km distance between the two meteorological towers because U at 40 m (measured at the 50 m tower) was on average higher than U at 80 m (measured at the 80 m tower), which resulted in average negative wind shear as seen in Figure 4(b). The meteorological towers and SODAR also were not co-located and were separated by a distance of 5 km between the 80 m tall tower and SODAR and nearly 6 km between the 50 m tower and farthest located SODAR position. These distances, across mildly hilly terrain, explain some of the discrepancy between the wind speed measurements.

The predominant wind direction at the wind farm was from the west-southwest from March through October whereas a bimodal wind direction distribution was observed from November to February with a primary peak in the west-southwest direction and a secondary peak in north-northeast. Wind direction histograms for 2 months, February and July, are shown in Figure 5 for three SODAR heights (40, 80 and 120 m) and are separated into nighttime and daytime periods to show both seasonal and temporal distributions. Eighty meter (hub height) winds were from the west-southwest over 85% of the time on July nights (Figure 5(e)) in contrast to 55% of the time on February nights (Figure 5(b)). During the daylight hours, 80 m winds were from the west-southwest 62% of the time in July whereas only 38% of the time in February. Overall,

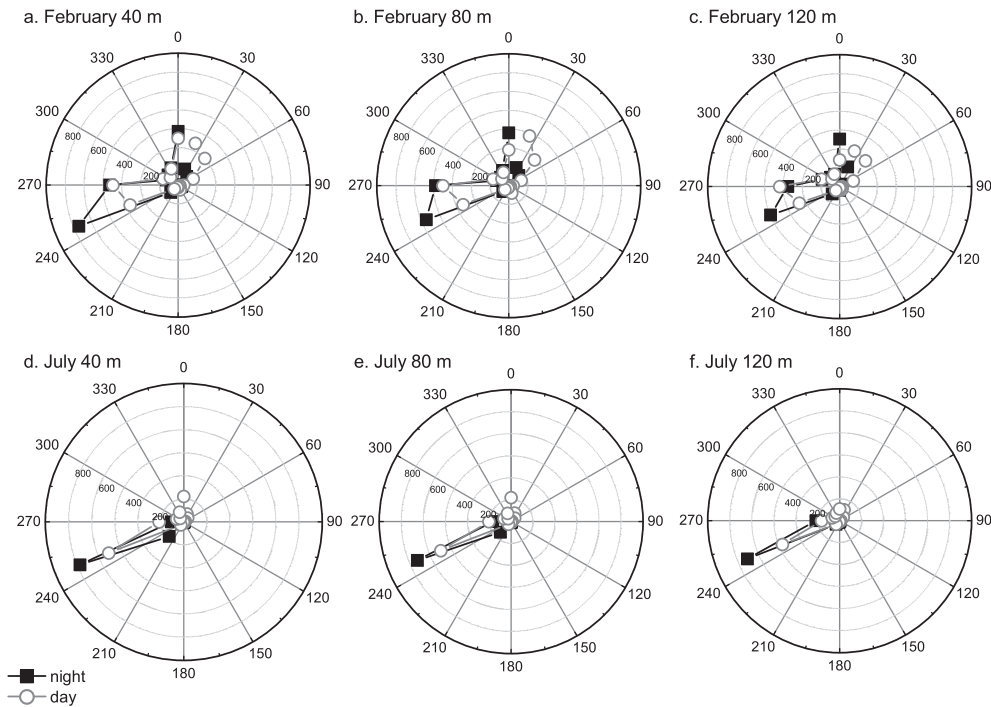


Figure 5. Frequency plots of nighttime/daytime wind direction for 40, 80 and 120 m wind speed during February (a–c) and July (d–f). Nighttime wind direction is predominately from the west-southwest in both months. During the winter, a secondary peak in daytime winds is observed from the northeasterly direction whereas during the summer, WSW winds dominate. Very little directional wind shear with height is evident regardless of month or time of day.

directional shear (change in wind direction with height) across heights representing the rotor disk was negligible, although greater shear was observed in February than in July. In contrast to wind speed in Figure 4, wind direction at the wind farm indicated only a small degree of temporal (night versus day) and spatial (vertical height and instrument location) variability during the peak power production summer months (Figure 5(d–f)).

3.2. Stability parameter analysis and comparison

Because of less data recovery in the rainy autumn/winter months and the occurrence of peak power production in the spring and summer months, all subsequent analysis concentrates on the warm season only. The percentage of spring- and summertime periods defined as stable (includes moderate and strong), neutral (includes weakly stable and weakly convective) or convective (includes moderate and strong) by the Obukhov length, wind shear exponent (across 40 to 120 m), horizontal turbulence intensity (at 80 m) and turbulence kinetic energy (at 80 m) are shown in Figure 6. The Obukhov length indicated stable : neutral : convective conditions in a 42:18:40 ratio with weakly stable and weakly convective regimes included in the neutral category (Figure 6(a)). As expected, daytime periods were primarily classified as strongly convective, convective or weakly convective, whereas nighttime periods were strongly stable, stable or slightly stable. Stable or very stable conditions were present on nearly every nighttime hour during the spring and summer months. The stability parameters, α_{40-120} (Figure 6(b)), $I_{U2SODAR}$ (Figure 6(e)) and TKE (Figure 6(f)) showed the highest agreement with L and predicted stable : neutral : convective ratios of 42:22:36, 40:20:40 and 42:20:38, respectively, whereas $I_{U_{cup}}$ (Figure 6(c)) and $I_{U1SODAR}$ (Figure 6(d)) under-predicted convective conditions by more than 10%.

Box-plot histograms of 10 min α (40 to 120 m), SODAR I_{U2} (80 m) and TKE (80 m) magnitudes according to z/L stability class are shown in Figure 7. The box plots show the mean, median, 25th and 75th percentiles for each stability parameter after bin averaging by z/L . Overall, there was high agreement between the derived stability parameters and the normalized Obukhov length. For example, when z/L indicated neutral conditions ($z/L \approx 0$), the median (25th percentile) (75th percentile) value for α_{40-120} was 0.14 (0.06) (0.23), $I_{U2SODAR}$ was 12.0% (9.7) (13.8), and TKE was $0.76 \text{ m}^2 \text{ s}^{-2}$ (0.54) (1.00). When z/L indicated stable conditions ($z/L > 0$), the median (25th percentile) (75th percentile)

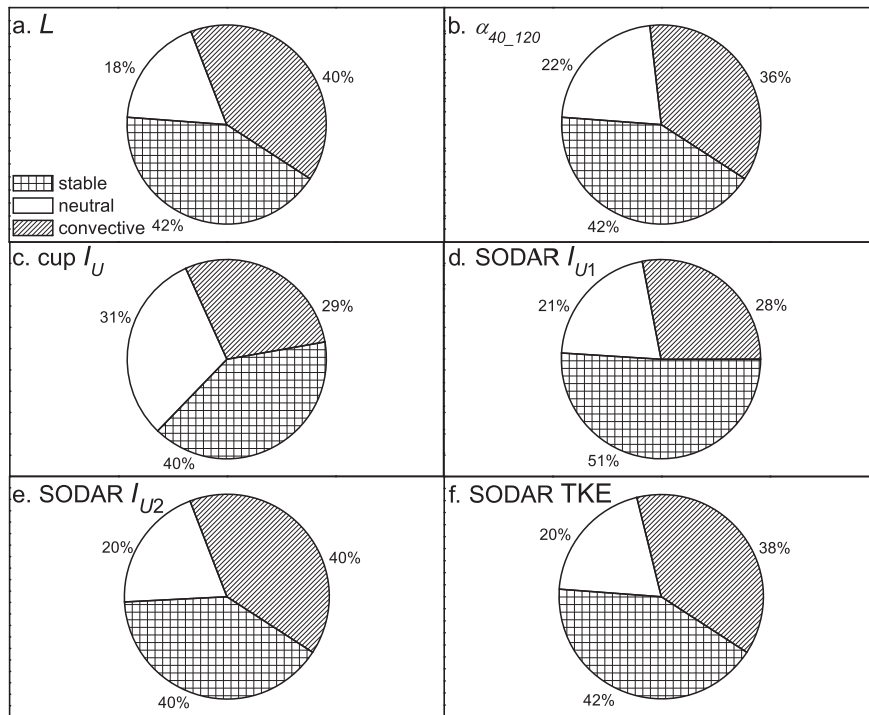


Figure 6. Percentage of spring and summer 10 min periods classified as stable, neutral or convective according to the stability parameters: (a) Obukhov length, (b) SODAR wind shear exponent, (c) cup anemometer I_U , (d) SODAR I_{U1} , (e) SODAR I_{U2} and (f) SODAR turbulence kinetic energy. I and TKE were measured at heights equivalent to hub height, whereas α represents heights across the entire rotor disk. The stability parameters with highest agreement to L are TKE and SODAR I_{U2} .

$\alpha_{40_120} = 0.31$ (0.24) (0.36), $I_{U2SODAR} = 8.2\%$ (7.3) (9.1), and $TKE = 0.42 \text{ m}^2 \text{ s}^{-2}$ (0.31) (0.55). When z/L indicated convective conditions ($z/L < 0$), the median (25th percentile) (75th percentile) $\alpha_{40_120} = 0.02$ (−0.04) (0.07), $I_{U2SODAR} = 24.2\%$ (17.2) (33.4), and $TKE = 1.20 \text{ m}^2 \text{ s}^{-2}$ (0.98) (1.38). The median values for α_{40_120} , $I_{U2SODAR}$ and TKE are well within the thresholds given in Table II for the three major stability regimes (stable, neutral and convective). Most of the 25th and 75th percentiles are also within the thresholds.

Mean diurnal patterns for the stability parameters during spring and summer are shown in Figure 8. In each panel, the gray shading indicates stable conditions, the ×-notched shading is neutral conditions and the white shading is convective conditions. Almost all of the stability parameters show distinctly stable conditions at night and convective conditions during the day. The normalized Obukhov length is shown for comparison with the on-site, derived stability parameters and shows that, on average, stable conditions existed from 19:00 to 05:00 Pacific Standard Time, neutral conditions occurred around sunrise and sunset and convective conditions were between 08:00 and 16:00 Pacific Standard Time (Figure 8(a)). Figure 8(b) shows the three SODAR wind shear exponents: α_{40_120} (shear across the entire rotor disk), α_{40_80} (shear across the lower half) and α_{80_120} (shear across the upper half), in comparison with the meteorological tower wind shear exponent, α_{50_80} (shear across the lower half). Diurnal wind shear variability was large and all four wind shear exponents were, on average, greater than 0.2 at night (indicating high shear and stable conditions) and less than 0.1 during the day (indicating low shear and convective conditions). Very high shear conditions ($\alpha = 0.3$ to 0.4) were consistently observed on spring and summer nights in the upper half of the rotor disk, possibly indicating the presence of LLJ structures at heights above the top blade tip, which did not penetrate to the lower half of the rotor. During the day, wind shear was generally highest in the lower half of the rotor disk (40 to 80 m) whereas α_{40_120} values indicated a well-mixed boundary layer across the entire swept area. Generally, magnitudes of SODAR α_{40_80} and cup anemometer α_{50_80} were very similar, as expected, although the cup anemometer indicated slightly less wind shear during the daylight hours.

Diurnal magnitudes of I_U indicated systematic instrument differences between the cup anemometer and SODAR as well as differences in the methodology used to calculate SODAR horizontal turbulence. $I_{U_{cup}}$ indicated, on average, higher turbulence intensities closer to the ground (50 vs 80 m) during both nighttime and daytime hours (Figure 8(c)). Mean cup anemometer I_U was 13.5% at 50 m and 12.7% at 80 m during midday hours and 9.7% at 50 m and 7.9% at 80 m at night. $I_{U_{50}}$ and $I_{U_{80}}$ were measured at different locations in the wind farm and are thus not directly comparable. The first SODAR-derived horizontal turbulence intensity, $I_{U1SODAR}$, showed a similar amount of diurnal variability as $I_{U_{cup}}$,

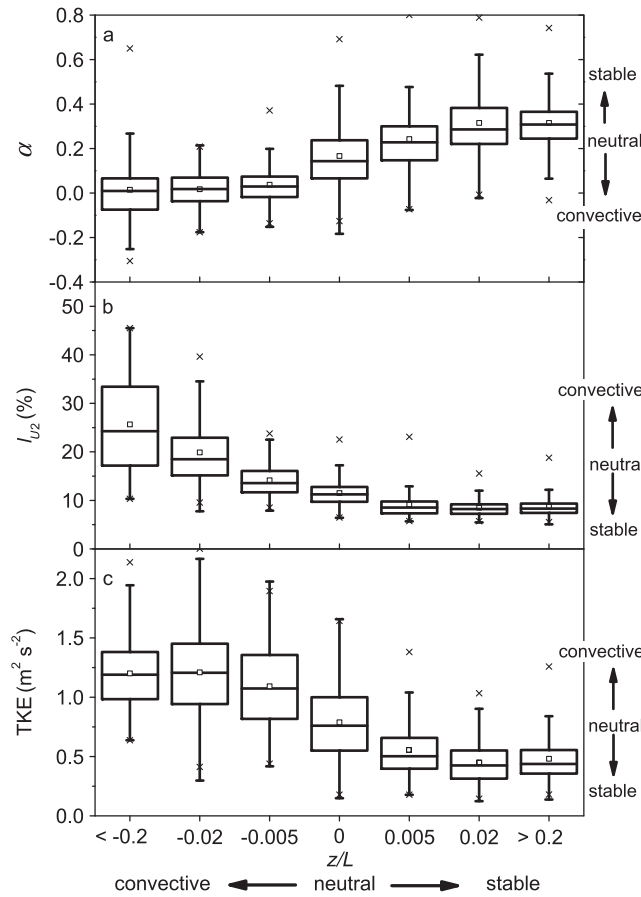


Figure 7. Box-plot histogram of 10 min (a) wind shear exponent (α_{40-120}), (b) hub-height turbulence intensity ($I_{U2SODAR}$) and (c) hub-height turbulence kinetic energy (TKE) data according to z/L stability class show good agreement between the three on-site SODAR stability parameters and the normalized Obukhov length. The box-plot histogram shows the mean (small square), median (horizontal line), 25th and 75th percentiles (bottom and top of the box), 5th and 95th percentiles (lower and upper whisker line) and 1st and 99th percentiles (x symbols).

although the SODAR parameter shows highest daytime I magnitudes at 120 m and highest nighttime I values at 40 m. Mean nighttime 40 m (80 m) (120 m) $I_{U1SODAR}$ was 7.6% (6.2%) (5.5%). Mean daytime 40 m (80 m) (120 m) $I_{U1SODAR}$ was 13.5% (14.4%) (14.8%). These differences with height and time of day are realistic given that turbulence at night is shear driven (e.g. friction along the surface), whereas daytime turbulence is dominated by large, buoyant eddies.

The second SODAR-derived I parameter, $I_{U2SODAR}$, showed a greater amount of diurnal variability than either I_{Ucup} or $I_{U1SODAR}$ and is shown in Figure 8(e). Hub-height $I_{U2SODAR}$ ranged from 20.3% during midday to 8.6% at night. $I_{U2SODAR}$ also showed slightly more stratification with height during the nighttime hours: mean $I = 10.8\%$ at 40 m and 7.7% at 120 m. The largest difference between hub-height I_{Ucup} , $I_{U1SODAR}$ and $I_{U2SODAR}$ magnitudes occurred during the daylight hours, and peak midday values ranged from 14.2% (I_{Ucup}) to 21.7% ($I_{U2SODAR}$). The cup anemometers systematically measured smaller turbulence intensities during the daylight hours as compared with SODAR. Further analysis showed that the instrument differences came largely from differences in the 10 min standard deviations (σ_U). Cup anemometer σ_U magnitudes were generally lower than both methods used to calculate SODAR σ_U . The square-root method (equation (8)) yielded up to 5% higher I_U magnitudes during the day than did the averaging method (equation (7)). A larger range of magnitudes made it possible to use $I_{U2SODAR}$ to distinguish very convective conditions from moderately convective.

The mean diurnal pattern for turbulence kinetic energy at heights of 40, 80 and 120 m appears in Figure 8(f). The degree of diurnal variability in TKE is very similar to that observed for $I_{U2SODAR}$. As with the SODAR I parameters, nighttime TKE decreased with height, whereas daytime TKE increased with height. Mean daytime (nighttime) TKE magnitudes were $1.60 \text{ m}^2 \text{ s}^{-2}$ ($0.63 \text{ m}^2 \text{ s}^{-2}$) at 120 m, $1.58 \text{ m}^2 \text{ s}^{-2}$ ($0.64 \text{ m}^2 \text{ s}^{-2}$) at 80 m and $1.42 \text{ m}^2 \text{ s}^{-2}$ ($0.71 \text{ m}^2 \text{ s}^{-2}$) at 40 m.

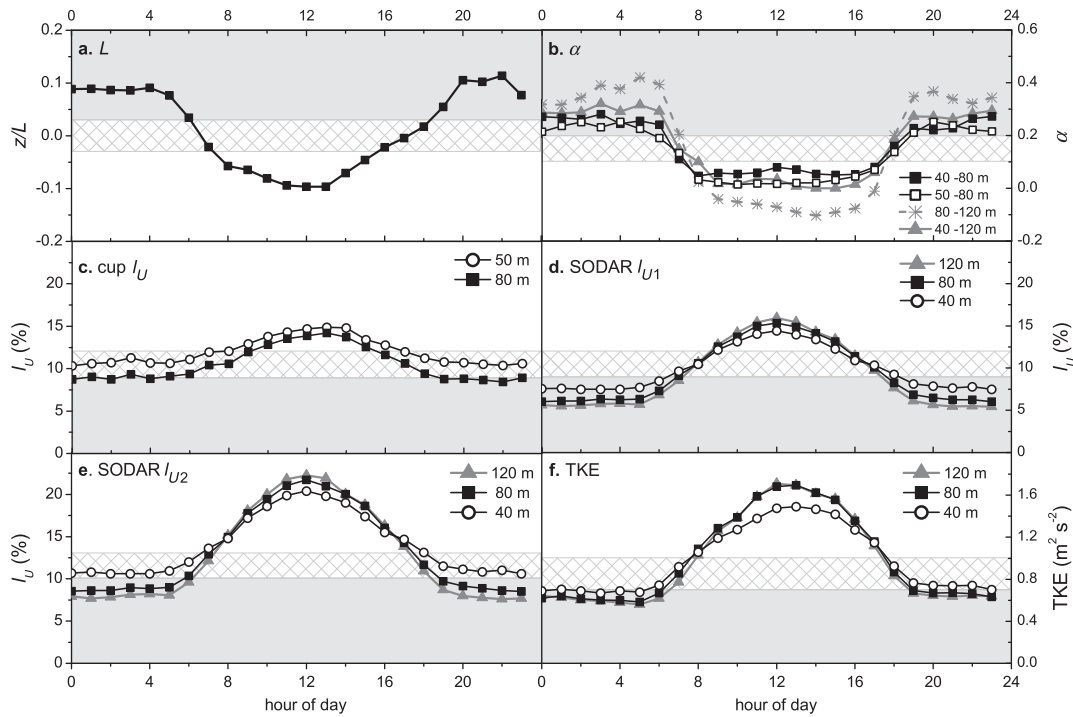


Figure 8. Mean diurnal plot of (a) the normalized Obukhov length, (b) wind shear exponent, (c) cup anemometer turbulence intensity, (d) SODAR turbulence intensity $I_{U1SODAR}$, (e) SODAR turbulence intensity $I_{U2SODAR}$ and (f) turbulence kinetic energy during the spring and summer months. All parameters show convective conditions during the day and stable conditions at night in agreement with z/L whereas $\alpha_{40,120}$, $I_{U2SODAR}$ and TKE show the highest amount of diurnal variability. The gray shading represents stable conditions, x-notched shading is neutral conditions and white shading is convective conditions according to the thresholds for each stability parameter as listed in Table II.

As expected, nighttime TKE magnitudes were indicative of stable, stratified flows, whereas daytime TKE showed a much more turbulent atmosphere.

3.3. Stability influence on wind velocity and turbulence profiles

The following sections use $I_{U2SODAR}$ (at 80 m) to quantify the effects of atmospheric stability on the rotor disk wind speed and turbulence profiles during spring and summer. Ten minute wind speeds at 40, 80 and 120 m were averaged by stability class in Figure 9 and are compared with seasonal averages. Stability-correlated variability was particularly high during the spring and summer months. Hub-height wind speed was significantly lower ($p < 0.05$) during convective or strongly convective conditions than during strongly stable, stable or neutral regimes. As expected, convective conditions showed almost no wind speed variability with height, whereas wind speeds were highly stratified across the rotor during stable and very stable conditions. Maximum wind speeds were observed during stable conditions, at all heights, with the largest stability-related differences occurring at the top of the rotor during the summer. For example, summer-time mean 120 m wind speed was 14.0 m s^{-1} during very stable conditions in comparison with 3.0 m s^{-1} during very convective conditions (Figure 9(b)).

Vertical profiles of wind speed and TKE at all heights across the rotor disk are shown in Figures 10 (for spring) and 11 (for summer) and are segregated according to stability class. Using wind speed observations at 80 m, and assuming an α value of $1/7$ in equation (2), we also calculated the power law wind speed profile. These figures show clear distinctions in how measured wind speed varies with height depending on atmospheric stability. Additionally, it is clear that a constant wind shear exponent is not sufficient in predicting the mean wind speed profile under non-neutral conditions.

In Figure 10(a), the power law inaccurately predicted wind speeds at the top and bottom of the rotor disk during both stable and convective conditions. For example, during stable conditions, the power law expression underestimated wind speed in the upper half of the rotor by 1 to 1.5 m s^{-1} and overestimated wind speed in the lower half by 0.5 to 1 m s^{-1} . While during convective conditions, the power law overestimated wind speed in the upper half of the rotor by 1.0 to 1.5 m s^{-1} and underestimated wind speed in the lower half by 0.3 m s^{-1} . In Figure 10(b), SODAR observations show that

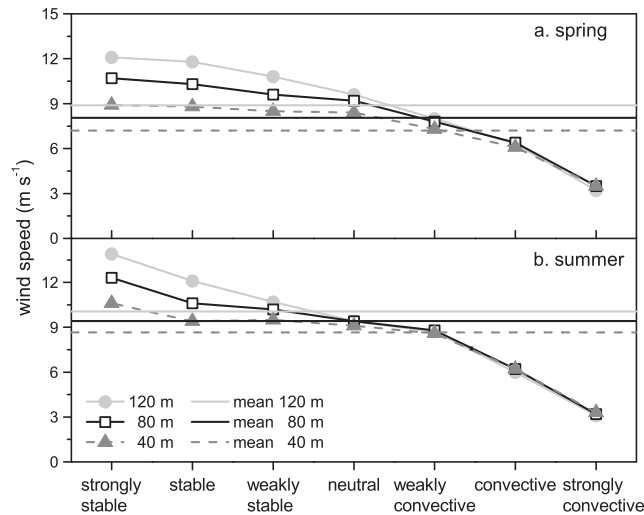


Figure 9. Mean wind speed at heights representative of the turbine rotor disk (40, 80 and 120 m) according to stability class in (a) spring and (b) summer. The largest stability influences occur during the summer season when strongly stable and strongly convective wind speeds differ by more than 10 m s^{-1} . The horizontal lines show the seasonal mean wind speed at each height.

TKE decreased with height (up to 100 m) during stable conditions, was nearly constant with height during near-neutral conditions and increased rapidly with height during convective conditions. The largest changes in TKE with height were observed in the lower half of the rotor, regardless of stability regime. A significant peak in TKE below the wind speed maxima ($\sim 130\text{--}150 \text{ m}$) was not noticeable during very stable conditions.

Summertime SODAR profiles of wind speed were similar to those observed in the spring, except that even stronger stability influences were observed during strongly stable and strongly convective conditions (Figure 11(a)). During strongly stable conditions, wind speed at the top of the rotor approached 14 m s^{-1} . This velocity was 1.5 m s^{-1} greater than the predicted wind speed at this height (using $\alpha = 1/7$), whereas in the lower half of the rotor, U was 10 m s^{-1} , a full meter per second slower than predicted with the power law. In contrast, during strongly convective conditions, the power law overestimated U in the top half of the rotor by 1.5 to 2.0 m s^{-1} and underestimated U in the lower half by 0.5 m s^{-1} . TKE profiles during the summer season are shown in Figure 11(b). Sharp increases in TKE with height were observed during convective conditions, whereas TKE was nearly constant with height during neutral and stable conditions. A slight peak in TKE was visible during very stable conditions at 140 m, which may indicate the presence of LLJs on summer nights (a wind maxima is also present at 150 m), although confirmation of LLJs is not possible without further investigation.

4. DISCUSSION

With the rapid expansion of wind farms and the significant penetration of wind energy into power markets, accurate estimates of wind power availability and the dependence of the wind resource on atmospheric boundary layer conditions, including stability, are required to assess wind plant performance. In this study, a unique data set from an onshore wind farm was explored to quantify the utility of various parameters of atmospheric stability, as well as document the impact of atmospheric stability on profiles of wind speed and turbulence across the rotor disk. In addition to typical wind farm meteorological tower and nacelle cup anemometers, this extensive data set included measurements from a remote-sensing SODAR and an off-site three-dimensional (3-D) sonic anemometer.

On average, wind farms in the contiguous USA produce maximum power in January and minimum power in August.⁶¹ In contrast, this wind farm exhibited maximum power output during the warmer months, with peak power produced on strongly stable spring and summer nights. The power season was largely driven by regional climatology. The climate includes a dry, warm season with strong thermal gradients and strong onshore flow, and a wet, cool season dominated by synoptic storms. The summertime peak in power coincided with higher wind speeds in the rotor disk, and in particular, with maximum wind speeds found at the top of the rotor (100 to 120 m) during stable nighttime conditions. The wintertime drop in power was due to fewer occurrences of strong, stable nighttime flows and an overall decrease in wind speeds at all heights within the rotor disk.

The on-site stability parameters α_{40-120} , $I_{U2SODAR}$ and TKE compared well with the sonic anemometer measurement of stability, L , whereas $I_{U_{cup}}$ and $I_{U1SODAR}$ tended to under-predict convective conditions. Previous wind farm studies

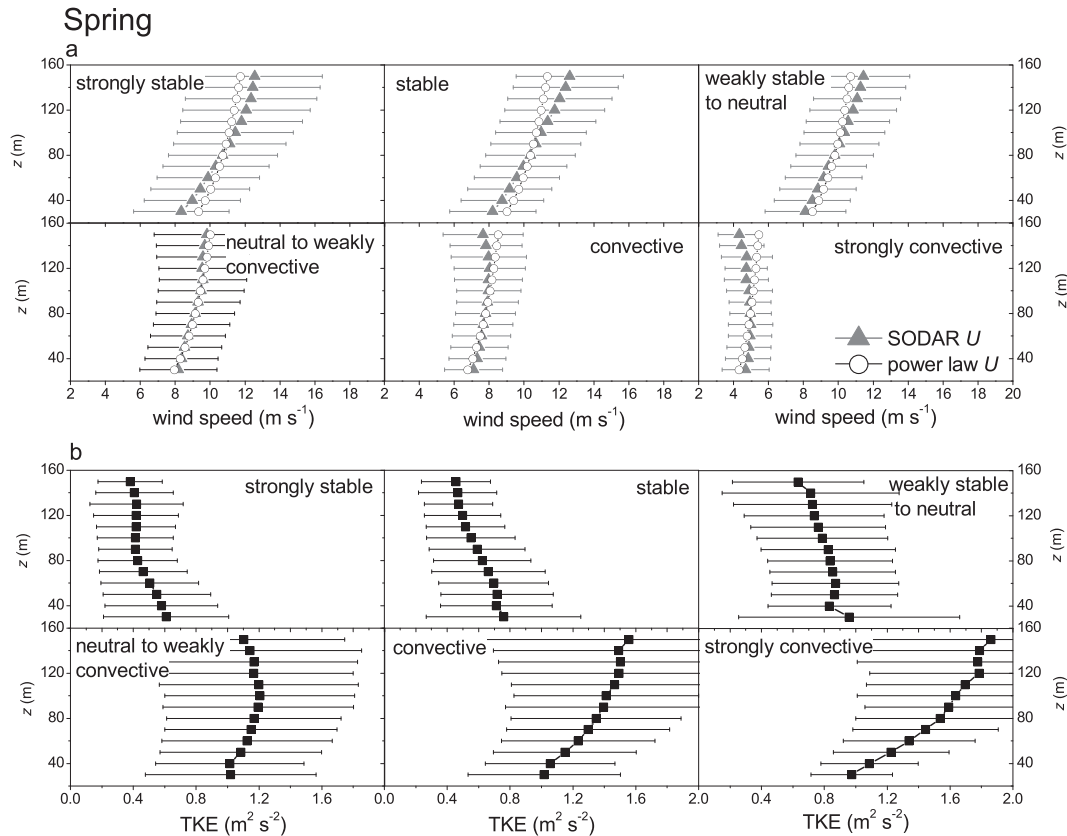


Figure 10. Spring vertical profiles (30 to 150 m) of SODAR (a) mean wind speed and (b) turbulence kinetic energy during strongly stable, stable, near-neutral, convective and strongly convective conditions. For reference, the turbine rotor disk covers heights of 40 to 120 m. The error bars are ± 1 standard deviation from the mean. Also plotted in (a) is the predicted wind speed profile (open circles) on the basis of the one-seventh power law ($\alpha = 0.14$) and the 80 m wind speed.

have determined stability on the basis of one or two of these parameters,^{5,8} whereas ours is the first study of our knowledge to compare such a large set of independent stability parameters. Observations of three-directional turbulence were available on site only because of the presence of the SODAR, although deployment of 3-D sonic anemometers on a tall meteorological tower could also enable quantification of TKE profiles. Along with power production and mean wind speed, stability regimes at our site were highly seasonal. The largest contrasts between stable and convective conditions appeared during thermally driven onshore flow in the spring and summer months.

We observed high amounts of wind shear across the rotor disk on summer nights in agreement with values found in other studies,^{30,62} indicating that the turbines at our site are, at times, above the atmospheric surface layer and are encountering complex, decoupled flow. Although all of the wind shear exponents characterized stability in agreement with L , we found that stability parameters that included information about turbulence from SODAR were slightly more accurate. Likewise, Sisterson and Frenzen⁶² found uncertainty with using wind shear to predict the mean wind speed profile, particularly during stable regimes.

Turbulence intensity magnitudes were very sensitive to the type of instrument used (cup anemometer versus SODAR) as well as to the methodology chosen to calculate horizontal turbulence when using a SODAR system. We calculated SODAR horizontal turbulence by using two methods. The first method used the average of the u and v fluctuations, whereas the second method used the square root of the sum of u and v fluctuations squared. The second calculation is used by micrometeorologists, whereas the first appears to be the primary method used in the wind energy industry. I observations presented here are comparable in magnitude with those of other wind energy studies^{6,30,31} when turbulence intensity was measured with either a cup anemometer or the averaging method ($I_{U1\text{SODAR}}$). In contrast, a larger range of horizontal turbulence intensity values was observed with the square-root method, and maximum $I_{U2\text{SODAR}}$ values exceed $I_{U\text{cup}}$ values published in the literature. This disparity can be attributed to a couple of factors: (i) the fluctuations in horizontal wind speed observed by SODAR were larger than those observed with the cup anemometers at this wind farm and (ii) the averaging

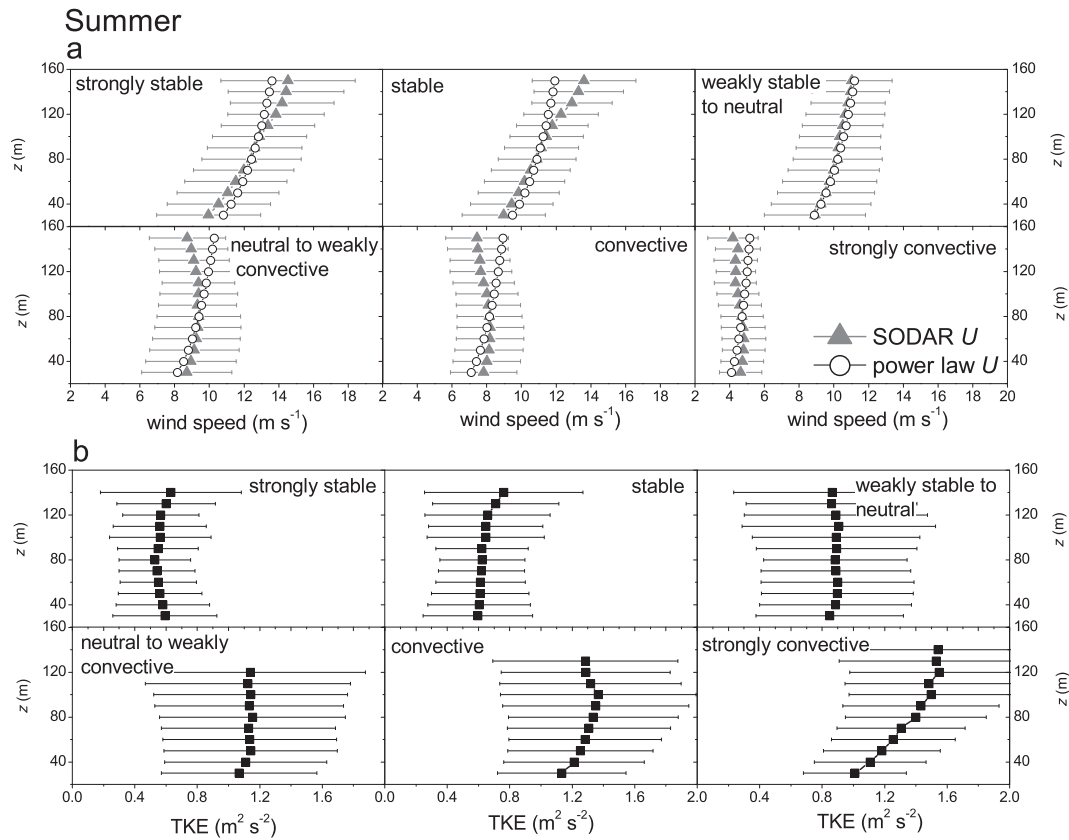


Figure 11. Summer vertical profiles (30 to 150 m) of SODAR (a) mean wind speed and (b) turbulence kinetic energy during strongly stable, stable, near-neutral, convective and strongly convective conditions. Also plotted in (a) is the predicted wind speed profile (open circles) on the basis of the one-seventh power law ($\alpha = 0.14$) and 80 m wind speed. Missing data are due to poor data recovery at those heights.

method used in calculating $I_{U1SODAR1}$ (equation 7) assumes that turbulence is isotropic and that fluctuations in the u and v velocities should be weighted equally, whereas the square-root method (equation (8)) makes no such assumptions. We believe that $I_{U2SODAR}$ is the best representation of the actual amount of turbulence present in the horizontal direction because it is a calculation of total, not average, horizontal turbulence. Moreover, the amount of diurnal variability in I_U resembled the diurnal variability in TKE, when $I_{U2SODAR}$ was chosen to represent horizontal turbulence intensity. Smaller amounts of diurnal variability in I_{Ucup} and $I_{U1SODAR}$ made it difficult to use these parameters to isolate two important stability classes: very stable from stable and very convective from convective.

Anemometer differences, including low variance in cup anemometer observations, also have been reported by Yahaya and Frangi⁶³ using controlled flow in wind tunnel experiments. We stress that cup anemometers are not suitable for making turbulence measurements because of their design. Cup anemometers respond faster to increases in velocity than to decreases,^{48,64} which can cause a typical cup anemometer to fail to measure 5% of the turbulent energy.⁶⁰ On the other hand, Wagner *et al.*³¹ also note a difference between SODAR and cup anemometer turbulence intensities and attribute it to the fact that SODAR measurements are noisy. Precipitation is a primary source of noise because sound can be scattered from raindrops back to the SODAR. Precipitation accounted for our lower SODAR data recovery rates during the autumn and winter months. In order to reduce this source of error from the SODAR data set, we removed moderate-to-high precipitation data points and focused our data analysis on the relatively dry spring and summer seasons.

In addition, there are fundamental differences in the way SODAR and cup anemometers measure wind speed, which may have led to the observed differences in I . SODAR measures vectors over a volume average whereas a cup anemometer does scalar averaging on a point measurement. Vector averaging can be up to 5% lower than scalar averaging, although the mean difference is around 2% to 3%.⁶⁵ Assuming equal variance between the two instruments, a lower wind speed would bias the SODAR I magnitudes towards greater values. SODAR systems also have error because of the fact that beam separation increases with height. These errors are on the order of 0% to 20%.⁶⁶ Furthermore, the equations used to calculate horizontal

wind speed from SODAR data assume a constant tilt angle between the latitudinal and longitudinal beams and the vertical acoustic beam and a non-zero vertical velocity. There is a chance that non-ideal conditions (e.g. non-flat terrain or the presence of strong buoyant thermals) at this wind farm caused small errors in σ_U , whereby some of the vertical velocity energy was 'miss-measured' as part of the horizontal wind speed. To reduce this potential bias in the SODAR data, so that we can more accurately describe the turbulence conditions at our site, we also calculated turbulence kinetic energy, which incorporates the velocity fluctuations in all three directions. If there is a bias in the horizontal components of turbulence because of the reasons described above, the error was removed by calculating a measure of total turbulence or TKE.

$I_{U2SODAR}$ did prove to be an accurate, on-site stability parameter for this wind farm as indicated by the high agreement with L and the significant correlations between wind speed and its derived stability regimes. Wind speed increased sharply with height during stable conditions, was nearly uniform or decreased slightly with height during convective conditions and was near-logarithmic under neutral conditions. Profiles of the 3-D turbulent kinetic energy also showed a strong dependency on atmospheric stability. During stable regimes, TKE decreased with height, indicating that turbulence was mechanically produced at the surface by friction. In contrast, during convective conditions, TKE sharply increased with height—convective eddies form near the surface and rise aloft and only the largest and most energetic eddies rise to higher altitudes. This behavior is consistent with that of the detailed investigations into the PBL.^{67–69} These stability profiles also agree with those of other wind power studies,^{27,31} which report that wind conditions differ above and below the turbine hub according to stability regime.

In very stable conditions, wind shear on the underside of an LLJ may produce intense, coherent, top-down forced turbulence.⁷⁰ This turbulence is transported downward by small-scale eddies. We found little evidence of turbulence produced aloft, such as a significant peak in TKE at the top of the rotor, although we did observe increasing wind speeds aloft (100 to 120 m), which indicated the possible presence of nocturnal LLJs. The lack of strong TKE maxima at the top of the nighttime profiles during very stable conditions may be due to several reasons. First, the downward transport of turbulence is, by nature, very intermittent¹⁴ and the instrument sampling frequency may have acted as a low-pass filter and missed these events. Second, LLJs could have occurred at heights above the maximum SODAR measurement height ($z > 200$ m). And finally, our seasonal averaging would eliminate evidence of LLJs if LLJs did not occur regularly each night.

It is our observation that wind speed and turbulence kinetic energy predictably vary with height depending on atmospheric stability. Therefore, there are numerous advantages to deploying sophisticated meteorological instruments at large wind farms, instead of relying on cup anemometers for sparse measurements of wind speed and turbulence intensity at hub height and possibly at one or more heights in the rotor disk. The high-resolution SODAR data confirmed that a constant wind shear exponent, as assumed by the power law, leads to grossly inaccurate predictions of wind speeds at the top and bottom of the rotor disk, particularly during strongly stable or strongly convective conditions. These inaccuracies can be either over-assessments of the wind resource (as seen in the turbulent periods at this site) or under-assessments of the wind resource (as seen in the stable periods at this site) and are consistent with findings in Sisterson *et al.*⁴⁵ Considering that the accuracy of wind speed across the entire rotor disk is critical to wind energy applications, we recommend that wind farms invest in more sophisticated meteorological instrumentation, such as remote-sensing platforms, which give high spatial-resolution velocity and turbulence measurements. Furthermore, our results strongly suggest that on-site, near-real-time estimates of stability would enable a wind farm to more accurately predict the available wind resource.

5. CONCLUSIONS

The main scientific conclusions that can be drawn from this study are:

- (1) Local atmospheric stability in the lower PBL can be quantified at wind farms in mildly complex terrain. Stability can be assessed by measuring wind shear across heights equal to the rotor disk or by measuring turbulence at heights equivalent to the rotor disk. Accurate measurements of turbulence require either a remote-sensing platform or sonic anemometer. Either hub-height equivalent turbulence intensity (using the square-root method) or turbulence kinetic energy can be used as a turbulence stability parameter, although TKE is theoretically superior to I because it is an absolute (not relative) measure of turbulence and includes all 3-D fluctuations in wind speed. We emphasize that all 3-D fluctuations in wind speed have the potential to impact wind turbine performance.
- (2) Vertical profiles of mean wind speed and turbulence across heights equivalent to the rotor disk are strongly correlated to atmospheric stability as seen in the high-resolution SODAR observations. Basing the available wind resource on hub-height wind speed without correcting for stability leads to either over-assessments of the wind resource during convective periods or under-assessments of the wind resource during stable regimes at this onshore wind farm.

ACKNOWLEDGEMENTS

We express great appreciation to Iberdrola Renewables, Inc. for the collection, provision and insightful discussion of this rich data set and, in particular, thank Dr. Justin Sharp, Dr. Mike Zulauf and Jerry Crescenti. Our gratitude goes to

John Wade, Neil Kelley and Dennis Elliott for their insightful reviews that improved this paper. We also acknowledge Dr. Dennis Baldocchi and Dr. Matteo Detto for their contribution of the sonic anemometer data (NSF-ATM-0628720) and Dr. Kyaw Tha Paw U for his expertise and advice regarding calculations of turbulence intensity. This work was funded by the Department of Energy's Wind and Water Power Program Office under the Renewable Systems Interconnect Support Program (BNR Code EB2502010), which is managed by Stan Calvert. LLNL is operated by Lawrence Livermore National Security, LLC, for the DOE, National Nuclear Security Administration under contract DE-AC52-07NA27344. NREL is a national laboratory of the US Department of Energy, Office of Energy Efficiency and Renewable Energy, operated by the Alliance for Sustainable Energy, LLC.

REFERENCES

1. DOE Wind and Water Power Program. *Wind power today* 2010. [Online]. Available: <http://www1.eere.energy.gov/windandhydro/pdfs/47531.pdf>. (Accessed 25 May 2010).
2. Enercon. World's most powerful wind turbine installed near Emden. *Windblatt Magazine* 2007; **4**: 6–7. [Online]. Available: <http://www.enercon.de/p/downloads/WB-0407-en.pdf>. (Accessed 16 May 2011).
3. Larsen SE, Gryning SE, Jensen NO, Jorgensen HE, Mann J. Mean wind and turbulence in the atmospheric boundary layer above the surface layer. In *Wind Energy, Proceedings of the Euromech Colloquium*, Peinke J, Schaumann P, Barth S (eds). Springer: Berlin, 2007; 21–25.
4. Elliott DL, Cadogan JB. Effects of wind shear and turbulence on wind turbine power curves, *Scientific Proceedings. European Community Wind Energy Conference and Exhibition*, Madrid, Spain, 1990.
5. Motta M, Barthelmie RJ, Vølund P. The influence of non-logarithmic wind speed profiles on potential power output at Danish offshore sites. *Wind Energy* 2005; **8**: 219–236.
6. Sumner J, Masson C. Influence of atmospheric stability on wind turbine power performance curves. *Journal of Solar Energy Engineering* 2006; **128**: 531–537.
7. Gottschall J, Peinke J. How to improve the estimation of power curves for wind turbines. *Environmental Research Letters* 2008; **3**: 1–7.
8. van den Berg GP. Wind turbine power and sound in relation to atmospheric stability. *Wind Energy* 2008; **11**: 151–169.
9. Antoniou I, Pedersen SM, Enevoldsen PB. Wind shear and uncertainties in power curve measurement and wind resources. *Wind Engineering* 2009; **33**: 449–468.
10. Tennekes H. Similarity relations, scaling laws and spectral dynamics. In *Atmospheric Turbulence and Air Pollution Modeling*. Reidel: Dordrecht, 1982; 37–68.
11. Blumen W, Banta R, Burns SP, Fritts DC, Newsom R, Poulos GS, Sun JL. Turbulence statistics of a Kelvin–Helmholtz billow event observed in the night-time boundary layer during the Cooperative Atmosphere–Surface Exchange Study Field. *Dynamics of Atmospheres and Oceans* 2001; **34**: 189–204.
12. Panofsky HA, Dutton JA. *Atmospheric Turbulence—Models and Methods for Engineering Applications*. John Wiley & Sons: New York, 1984; 397 pp.
13. Kaimal JC, Finnigan JJ. *Atmospheric Boundary Layer Flows—Their Structure and Measurement*. Oxford University Press: New York, 1994; 287 pp.
14. Mahrt L, Sun J, Blumen W, Delany T, Oncley S. Nocturnal boundary-layer regimes. *Boundary-Layer Meteorology* 1998; **88**: 255–278.
15. Mahrt L. Stratified atmospheric boundary layers. *Boundary-Layer Meteorology* 1999; **90**: 375–396.
16. Mahrt L, Vickers D. Contrasting vertical structures of nocturnal boundary layers. *Boundary-Layer Meteorology* 2002; **105**: 351–363.
17. Stull RB. *An Introduction to Boundary Layer Meteorology*. Kluwer Academic Publishers: Dordrecht, 1988; 670 pp.
18. Joffre SM. Power laws and the empirical representation of velocity and directional shear. *Journal of Climate and Applied Meteorology* 1984; **12**: 1196–1203.
19. Heald RC, Mahrt L. The dependence of boundary-layer shear on diurnal variation of stability. *Journal of Applied Meteorology* 1981; **20**: 859–867.
20. Kelley ND, Osgood RM, Bialasiewicz JT, Jakubowski A. Using wavelet analysis to assess turbulence/rotor interactions. *Wind Energy* 2001; **3**: 121–134.
21. Hand MM, Kelley ND, Balas MJ. Identification of wind turbine response to turbulent inflow structures. *NREL/CP-500-33465*, 2003.

22. Blackadar AK. Boundary layer wind maxima and their significance for the growth of nocturnal inversions. *Bulletin of the American Meteorological Society* 1957; **38**: 283–290.
23. Banta RM. Stable-boundary-layer regimes from the perspective of the low-level jet. *Acta Geophysica* 2008; **56**: 58–87.
24. Kelley ND, Shirazim M, Jager D, Wilde S, Adams J, Buhl M, Sullivan P, Pattonm E. Lamar low-level jet project interim report. *NREL/TP-500-34593*, Golden, CO, National Renewable Laboratory, 2004. 216 pp.
25. Emeis S, Harris M, Banta RM. Boundary-layer anemometry by optical remote sensing for wind energy applications. *Meteorologische Zeitschrift* 2007; **16**: 337–347.
26. Cosack N, Emeis S, Kuhn M. On the influence of low-level jets on energy production and loading of wind turbines. In *Wind Energy, Proceeding of the Euromech Colloquium*, Peinke J, Schaumann P, Barth S (eds). Springer: Berlin, 2007; 325–328.
27. Pichugina YL, Banta RM, Kelley ND, Brewer WA, Sandberg SP, Machol JL, Jonkman BJ. Remote sensing of the nocturnal boundary layer for wind energy applications. 14th International Symposium for the Advancement of Boundary Layer Remote Sensing, Conference Series. *Earth and Environmental Science* 2008; **1**. DOI: 10.1088/1755-1307/1/1/012048.
28. Storm B, Dudhia J, Basu S, Swift A, Giammanco I. Evaluation of the weather research and forecasting model on forecasting low-level jets: implications for wind energy. *Wind Energy* 2009; **12**: 81–90.
29. Hunterm R, Pedersen TF, Dunbabin P, Antoniou A, Frandsen S, Klug H, Albers A, Lee WK. European wind turbines testing procedure developments task 1: measurement method to verify wind turbine performance characteristics. *RISØ R-1209(EN)*, Risø National Laboratory, Roskilde, 2001. 120 pp.
30. Rareshidem E, Tindal A, Johnson C, Graves AM, Simpson E, Blegg J, Harris T, Schoborg D. Effects of complex wind regimes on turbine performance, *Scientific Proceedings. American Wind Energy Association WINDPOWER Conference*, Chicago, IL, 2009.
31. Wagner R, Antoniou I, Pedersen SM, Courtney MS, Jørgensen HE. The influence of the wind speed profile on wind turbine performance measurements. *Wind Energy* 2009; **12**: 348–362.
32. Kaiser K, Hohlen H, Langreder W. Turbulence correction for power curves, *Scientific Proceedings. European Wind Energy Conference and Exhibition*, Madrid, Spain, 2003.
33. Honhoff S. Power curves—the effect of environmental conditions, *Scientific Proceedings. GE Wind, AWEA Wind Speed and Energy Workshop*, Portland, OR, 2007.
34. Tindal A, Johnson C, LeBlanc M, Harman K, Rareshide E, Graves A-M. Site-specific adjustments to wind turbine power curves, *Scientific Proceedings. American Wind Energy Association WINDPOWER Conference*, Houston, TX, 2008.
35. International Electromechanical Commission (IEC). Wind turbines—part 12-1: power performance measurements of electricity producing wind turbines. *Technical Report No. IEC 61400-12-1*, 2005.
36. Coulter RL, Kallistratova MA. The role of acoustic sounding in a high-technology era. *Meteorology and Atmospheric Physics* 1999; **71**: 3–13.
37. Crescenti GH. A look back on two decades of Doppler sodar comparison studies. *Bulletin of the American Meteorological Society* 1997; **78**: 651–673.
38. Antoniou I, Jørgensen HE, Ormel F, Bradley S, von Hünerbein S, Emeis S, Warmbier G. *On the Theory of SODAR Measurement Techniques*. Risø, National Laboratory: Roskilde, Denmark, 2003; 9 pp.
39. Sutton OG. *Atmospheric Turbulence*. Methuen & Co. Ltd: London, 1949; 107 pp.
40. Elliott DL, Holliday C, Barchet W, Foote H, Sandusky W. *Wind Energy Resource Atlas of the United States*. DOE/CH 10093-4. Golden, Colorado: Solar Energy Research Institute, 1987. 210 pp.
41. Rohatgi J. An analysis of the influence of atmospheric stability on vertical wind profiles—its influence on wind energy and wind turbines. *Wind Engineering* 1996; **20**: 319–332.
42. Scrase FJ. Some characteristics of eddy motion in the atmosphere. Meteorological Office. *Geophysical Memoir* 1930; **52**.
43. Justus CG, Mikhail A. Height variation of wind speed and wind distributions statistics. *Geophysical Research Letters* 1976; **3**: 261–264.
44. Peterson EW, Hennessey JP. On the use of power laws for estimates of wind power potential. *Journal of Applied Meteorology* 1977; **17**: 390–394.
45. Sisterson DL, Hick BB, Coulter RL, Wesely ML. Difficulties in using power laws for wind energy assessment. *Solar Energy* 1983; **31**: 201–204.

46. Shaw RH, Hartog GD, King KM, Thurtell GW. Measurements of mean wind flow and three-dimensional turbulence intensity within a mature corn canopy. *Agricultural Meteorology* 1974; **13**: 419–425.
47. Chan PW. Measurement of turbulence intensity profile by a mini-sodar. *Meteorological Applications* 2008; **15**: 249–258.
48. Weber RO. Estimators for the standard deviations of lateral, longitudinal, and vertical wind components. *Atmospheric Environment* 1998; **32**: 3639–3646.
49. Piper M, Lundquist JK. Surface layer turbulence measurements during a frontal passage. *Journal of the Atmospheric Sciences* 2004; **61**: 1768–1780.
50. Mahrt L, Vickers D, Nakamura R, Soler MR, Sun J, Burns S, Lenschow DH. Shallow drainage flows. *Boundary-Layer Meteorology* 2001; **101**: 243–260.
51. Lundquist JK. Intermittent and elliptical inertial oscillations in the atmospheric boundary layer. *Journal of the Atmospheric Sciences* 2003; **60**: 2661–2673.
52. Lundquist JK, Mirocha JD. Interaction of nocturnal low-level jets with urban geometries as seen in Joint Urban 2003 data. *Journal of Climate and Applied Meteorology* 2008; **47**: 44–58.
53. Monin AS, Obukhov AM. Basic laws of turbulent mixing in the ground layer of the atmosphere. *Transactions of the Institute of Geophysics, USSR* 1954; **151**: 163–187.
54. Obukhov AM. Turbulence in an atmosphere with a non-uniform temperature. *Boundary-Layer Meteorology* 1971; **2**: 7–29.
55. Nieuwstadt FTM. The turbulent structure of the stable, nocturnal boundary layer. *Journal of the Atmospheric Sciences* 1984; **41**: 2202–2216.
56. van Wijk AJM, Beljaars ACM, Holtslag AAM, Turkenburg WC. Evaluation of stability corrections in wind speed profiles over the North Sea. *Journal of Wind Engineering & Industrial Aerodynamics* 1990; **33**: 551–566.
57. Sathe A, Bierbooms W. Influence of different wind profiles due to varying atmospheric stability on the fatigue life of wind turbines. *Journal of Physics: Conference Series* 2007; **75**: 1–7.
58. Walter K, Weiss CC, Swift A, Chapman J, Kelley ND. Speed and direction shear in the stable nocturnal boundary layer. *Journal of Solar Energy Engineering* 2009; **131**: 1–7.
59. Langreder W, Højstrup J, Kaiser K, Hohlen H. Turbulence correction for power curves, *Scientific Proceedings. European Wind Energy Conference and Exhibition*, London, 2004.
60. Pedersen BM, Pedersen TF, Klug H, van der Borg N, Kelley N, Dahlberg JA. Wind speed measurement and use of cup anemometry. In *Recommended Practices for Wind Turbine Testing and Evaluation*, Hunter RS (ed.). IEA: Paris, 1999; 49 pp.
61. Lu X, McElroy MB, Kiviluoma J. Global potential for wind-generated electricity. *Proceedings of the National Academy of Sciences* 2009; **106**: 10933–10938.
62. Sisterson DL, Frenzen P. Nocturnal boundary-layer wind maxima and the problem of wind power assessment. *Environmental Science & Technology* 1978; **12**: 218–221.
63. Yahaya S, Frangi JP. *Spectral Response of Cup Anemometers*. Laboratoire Environnement et Développement Report 2003: 1–3.
64. Hölling M, Schulte B, Barth S, Peinke J. Sphere anemometer—a faster alternative solution to cup anemometry. The science of making torque from wind. *Journal of Physics: Conference Series* 2007; **75**: 012064.
65. Moore KE, Bailey BH. *Recommended practices for the use of SODAR in wind energy resource assessment*. Integrated Environmental Data, LLC 2009: 1–13.
66. von Hünerbein S, Antoniou I, Bradley SG, Jørgensen HE, Kindler D. Calibration of SODARs for wind energy applications, *International Symposium for the Advancement of Boundary Layer Remote Sensing*, Garmisch-Partenkirchen (Germany), 2006.
67. Hicks BB. Wind profile relationships from the ‘Wangara’ experiment. *Quarterly Journal of the Royal Meteorological Society* 1976; **102**: 535–551.
68. André J-C, De Moor G, Lacarrère P, Therry G, du Vachat R. Modeling the 24-hour evolution of the mean and turbulent structure of the planetary boundary layer. *Journal of the Atmospheric Sciences* 1978; **35**: 1861–1883.
69. Poulos GS, Blumen W, Fritts DC, Lundquist JK, Sun J, Burns SP, Nappo C, Banta R, Newsom R, Cuxart J, Terradellas E, Balsley B, Jensen M. CASES-99: a comprehensive investigation of the stable nocturnal boundary layer. *Bulletin of the American Meteorological Society* 2002; **83**: 555–581.
70. Smedman A-S. Observations of a multi-level turbulence structure in a very stable atmospheric boundary layer. *Boundary-Layer Meteorology* 1988; **44**: 231–253.